On the electrical energy consumption of active ankle prostheses with series and parallel elastic elements

Verstraten, Tom; Flynn, Louis; Geeroms, Joost; Vanderborght, Bram; Lefeber, Dirk

Published in:
BIOROB 2018 - 7th IEEE International Conference on Biomedical Robotics and Biomechatronics

DOI:
10.1109/BIOROB.2018.8487656

Publication date:
2018

Document Version:
Accepted author manuscript

On the electrical energy consumption of active ankle prostheses with series and parallel elastic elements

Tom Verstraten[1], Louis Flynn[1], Joost Geeroms[1], Bram Vanderborght[1] and Dirk Lefeber[1]

***Abstract*— With series and parallel elastic elements, considerable reductions in the mechanical peak power and energy consumption of active ankle prostheses can be obtained. Very few works, however, evaluate the electrical energy consumption of these devices. In this work, we analyze and discuss the differences between the mechanical and electrical energy consumption of these actuators. Design optimizations based on mechanical and electrical energy consumption are compared for a series elastic actuator, parallel elastic actuator and series elastic actuator with unidirectional spring. The results are then analyzed by means of torque-angle plots, power flow graphs and motor efficiency maps. The analysis highlights the impact of drivetrain inertia on the peak power and energy efficiency of the system. Moreover, interaction between the series spring and unidirectional parallel spring is identified as a potential cause of reduced actuator bandwidth. A parallel elastic actuator is found to be the most compact and energy-efficient solution overall as it makes the most efficient use of the electric motor.**

I. Introduction

Energy consumption is crucial in wearable robotics, where the user not only needs to carry the actuators, but also its power supply. The energy consumption of actuators performing cyclic motions can be decreased by using elastic elements [1]. The principle is sketched in Fig. 1. In a rigid actuator (Fig. 1a), energy is dissipated in the drivetrain components when power flows through them. In elastic actuators, such as the SEA depicted in Fig. 1b, the elastic element – which is an energy buffer – enables direct power exchange with the load. As a result, the power flow through the actuator is reduced, and so are the losses.

Because of their energy efficiency, elastic actuators are commonly used in several designs of active ankle prostheses. Both Series Elastic Actuators (SEAs) [2], [3] and Parallel Elastic Actuators (PEAs) [4], [5] have been implemented in state-of-the art active prostheses. In some cases, the two principles are combined in a single actuator to achieve even greater benefits [6], [7].

Very often, inverse dynamic optimizations based on mechanical energy consumption or peak power [8], [9], [10], [11] are used to optimize the springs in elastically actuated prosthesis designs. Although these optimizations give very important insights regarding the role of parallel and series elastic elements, there are several issues with this approach. Firstly, motor inertia is not taken into account. This can have a distinct effect on the optimized spring stiffness. For example, if the design of a SEA-driven prosthetic knee is optimized for peak power, an infinite stiffness would be found as the optimal solution if the actuator inertia is considered, whereas a finite stiffness is found if it is included [12]. Secondly, motor limitations are not taken into account, although these ultimately determine the actuator's work output and bandwidth [13]. It has been shown that the smallest possible motor for a SEA-driven ankle prosthesis would saturate if the springs were chosen based on an inverse dynamic optimization in which motor limitations are not taken into account [14]. The authors of this work have therefore suggested selecting the springs in function of the motor's limitations. They demonstrated that, with such an approach, the optimal actuator for an active ankle prosthesis would be a PEA with unidirectional parallel spring [15]. A series spring can be added for shock tolerance, but would need to be as stiff as possible. This principle was applied in the BiOM prosthesis [6].

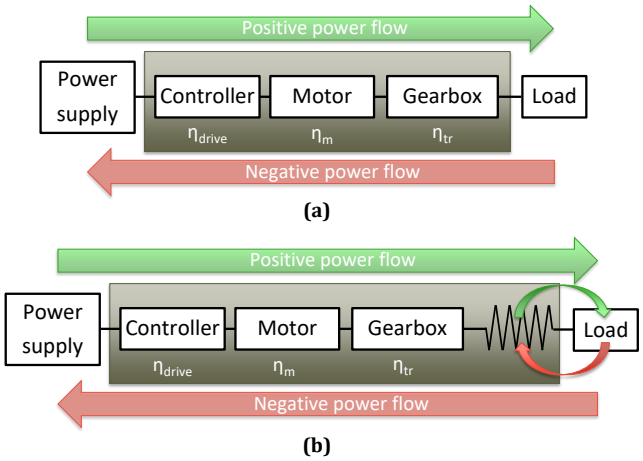

Fig. 1: Power flows in (a) a rigid actuator and (b) a Series Elastic Actuator.

In this paper, we study the effects of parallel and series elastic elements on an active ankle prosthesis. Its power and energy consumption are evaluated in the electrical domain as well as in the mechanical domain. The paper is structured as follows. In Section II, we present the methods used for the optimization. In Section III, we present the results of optimization of an SEA, PEA and SEA with additional unidirectional parallel spring. We interpret these results by means of their power flows, torque-angle characteristics and

All authors are with the Robotics & Multibody Mechanics Research Group (R&MM), Faculty of Mechanical Engineering, Vrije Universiteit Brussel and Flanders Make, Pleinlaan 2, 1050 Elsene, Belgium

Part of this work was funded by the European Commission ERC Starting grant SPEAR (no. 337596) and CYBERLEGs PlusPlus (H2020-ICT-2016-1 Grant Agreement #731931)

[1]Corresponding author: Tom.Verstraten@vub.be

motor efficiency maps. The advantages and disadvantages of inverse dynamic optimizations based on mechanical and electrical energy consumption are discussed in Section IV. The main findings are summarized in Section V.

II. Methods

The optimizations presented in this work rely on inverse dynamics, i.e., we assume that the required ankle torque T and ankle position θ perfectly match the biological ankle data from Winter for an able-bodied person of 75 kg [16]. The gear ratio, the stiffness of the series and/or the unidirectional parallel spring and the equilibrium angle of the latter are optimized by means of a parameter sweep within a reasonable range of values.

A. Equations

The torque on the gearbox T_l is the sum of the required output torque T and the parallel spring torque T_s:

$$T_l = T + T_s \tag{1}$$

The torque provided by the unidirectional parallel spring is

$$T_s = \begin{cases} k_p\left(\theta - \theta_{eq}\right) & \left(\theta \geq \theta_{eq}\right) \\ 0 & \left(\theta < \theta_{eq}\right) \end{cases} \tag{2}$$

Equation (2), however, is not differentiable at angle $\theta = \theta_{eq}$. For this reason, we use following alternative which is differentiable for any θ:

$$T_s = k_p\left(\theta - \theta_{eq} + \frac{1}{2}\sqrt{s^2 + \left(\theta - \theta_{eq}\right)^2}\right) \tag{3}$$

The lower the value of the smoothing factor s, the more (3) will resemble (2). In this work, s = 0.01 rad^{-1} was deemed to yield realistic results.

The torque on the motor shaft T_m is given by

$$T_m = \frac{C}{n} T_l \tag{4}$$

where n stands for the gear reduction ratio. C is the gearbox efficiency function, derived from the datasheet efficiency η_{tr}:

$$C = \begin{cases} 1/\eta_{tr} & \left(P_{mech} > 0\right) \\ \eta_{tr} & \left(P_{mech} < 0\right) \end{cases} \tag{5}$$

with $P_{mech} = T_l \dot{\theta}_m$ the mechanical power. From Hooke's law, we can derive the expression which links motor speed $\dot{\theta}_m$ to series spring stiffness k_s:

$$\dot{\theta}_m = n \cdot \left(\dot{T}_l / k_s + \dot{\theta}\right) \tag{6}$$

In a PEA, $\dot{\theta}_m = \dot{\theta}$. Finally, we apply the DC motor model

$$\begin{cases} I = \frac{1}{k_t}\left(\left(J_m + J_{tr}\right)\ddot{\theta}_m + T_m + \nu_m \dot{\theta}_m\right) \\ U = L\dot{I} + RI + k_t \dot{\theta}_m \end{cases} \tag{7}$$

in order to find the voltage U and current I at the motor terminals. This model includes both Joule losses RI^2 and speed-dependent losses $\nu_m \dot{\theta}_m^2$. The latter term is an accurate representation of viscous friction and Eddy current losses. The electrical power consumption P_{elec} is then found by multiplying motor current and voltage. The parameters in (7) are defined in Table I, as well as the values for the two motors and the gearbox used in this work.

	RE40 (150 W)	RE50 (200 W)
Part number	148867	370354
Torque constant k_t (mNm/A)	30.2	38.5
Friction coefficient ν_m (Nms/rad)	5.21e-6	1.46e-5
Terminal resistance R (Ω)	0.299	0.103
Terminal inductance L (mH)	0.0823	0.072
Motor inertia J_m (gcm²)	142	536
Max. speed $\dot{\theta}_{max}$ (rpm)	12 000	9 500
Max. continuous torque $T_{m,max,cont}$ (mNm)	177	405
Max. peak current $I_{m,max}$ (A)	23.4	30
Motor efficiency η_m	91%	94%
Gearbox inertia J_{tr} (gcm²)	16.5	
Gearbox efficiency η_{tr}	68 %	

TABLE I: Properties of the motors and gearbox used in the optimization.

B. Constraints

The optimization is subject to the constraints

$$\left|\dot{\theta}_m\right| < \dot{\theta}_{max} \tag{8}$$

$$\left[k_t I\right]_{RMS} < T_{m,max,cont} \tag{9}$$

$$\left|I_m\right| < I_{m,max} \tag{10}$$

$$\left|T_m + \left(J_m + J_{tr}\right)\ddot{\theta}_m + \left(\nu + \frac{k_b k_t}{R}\right)\dot{\theta}_m\right| < U_{max}\frac{k_T}{R} \tag{11}$$

which limit the motor speed, rms torque, peak current and motor voltage. The maximum values $\dot{\theta}_{max}$, $T_{m,max,cont}$ and $I_{m,max}$ depend on the selected drivetrain, and are given in Table I. For the maximum voltage U_{max}, we select 48 V.

C. Optimization objectives

1) Minimal mechanical energy consumption (MEC): Mechanical energy consumption is typically calculated as

$$E_{mech,abs} = \int \left|P_{mech}\right| dt \tag{12}$$

Equation (12) does, however, not represent the actual mechanical energy consumption – it should be calculated without absolute value. Instead, it is a measure of the average power flow through the actuator. The general idea is that, if power loss is assumed to be proportional to the power flowing through the actuator's components, (12) minimizes the overall energy consumption. Different components of the actuator however have different loss mechanisms which, along with the inertia of the drivetrain, could have a distinct impact on the optimization [17]. These are not accounted for in this simplified cost function.

In the MEC optimization, the motor constraints specified in section II-B are not taken into account, in accordance with prior works by Grimmer et al. [9], [8] and Eslamy et al. [10].

2) Minimal electrical energy consumption (EEC): Electrical energy consumption is given by

$$E_{elec} = \int P_{elec} dt \tag{13}$$

This equation represents the energy at the motor terminals. Motor constraints are taken into account in accordance with section II-B.

	Rigid actuation	MEC	EEC
k_s	∞	382 Nm/rad	330 Nm/rad
$\lvert P_{mech}\rvert$	252 W	112 W	130 W
$\lvert P_{elec}\rvert$	(615 W)	(298 W)	281 W
$E_{mech,abs}$	35.4 J	19.6 J	21.6 J
E_{elec}	(47.3 J)	(40.7 J)	40.7 J
n	(150)	(250)	248

(a) SEA (with 200W Maxon motor)

	Rigid actuation	MEC	EEC
k_p	0	632 Nm/rad	564 Nm/rad
θ_{eq}	N/A	-1°	-1°
$\lvert P_{mech}\rvert$	252 W	213 W	206 W
$\lvert P_{elec}\rvert$	(615 W)	(470.2 W)	450 W
$E_{mech,abs}$	35.4 J	20.0 J	20.1 J
E_{elec}	(64.3 J)	(36.2 J)	36.0 J
n	(375)	(257)	251

(b) PEA (with 150W Maxon motor)

	Rigid actuation	MEC	EEC
k_s	∞	380 Nm/rad	2000 Nm/rad
k_p	0	0 Nm/rad	590 Nm/rad
θ_{eq}	N/A	N/A	-1°
$\lvert P_{mech}\rvert$	252 W	113 W	220 W
$\lvert P_{elec}\rvert$	(615 W)	(312 W)	463 W
$E_{mech,abs}$	35.4 J	19.6 J	20.3 J
E_{elec}	(64.3 J)	(45.8 J)	35.5 J
n	(375)	(467)	246

(c) SEA+UPS (with 150W Maxon motor)

TABLE II: Optimization of an SEA (series spring stiffness k_s), PEA with unidirectional parallel spring (stiffness k_p, equilibrium angle θ_{eq}) and SEA+UPS (SEA with unidirectional parallel spring) for an active ankle prosthesis. Optimization criteria are mechanical energy consumption (MEC) and electrical energy consumption (EEC). Peak powers and energy consumption of a rigid actuator is shown for reference. Values in brackets indicate that the results violate one or more motor constraints.

III. Optimization of spring stiffness

A. Optimization results

Table II shows the results of the optimizations for the MEC and EEC criteria for the SEA, PEA and SEA with unidirectional parallel spring (SEA+UPS). For the electrical calculations, the smallest motor was selected that enables perfect tracking of the imposed output trajectory, i.e. that respects all constraints in the inverse dynamic calculations. As indicated in the table, a 200 W motor was selected for the SEA case, while a 150 W motor appeared to be sufficient for the PEA and SEA+UPS case. This illustrates the claim that parallel springs allow for a greater reduction of motor size and/or gear ratio [11]. In this optimization, the optimal gear ratios for the SEA, PEA and SEA+UPS in the EEC optimization turned out to be the same.

As motor constraints were not taken into account for the MEC optimization, the results from this optimization send the motor into saturation. This was also remarked and discussed in [15]. The values for electrical energy consumption presented in Table II are therefore only indicative. In reality, saturation will cause the electrical energy consumption and peak power to be lower, although this decrease is the result of a decrease in mechanical power supplied to the output rather than a gain in efficiency.

Another interesting observation is that the SEA+UPS optimization eliminates the parallel spring in the MEC optimization ($k_p = 0$) and the series spring in the EEC optimization (k_s reaches maximum). In other words, solutions where both springs are combined will not only lead to a larger design with more components; they will also not lead to a decrease in energy consumption. To understand this result, we present a power flow analysis in the following subsection.

B. Power flow analysis

Four important power flows are represented in Fig. 2 for the MEC optimization of the SEA (Fig. 2a) and PEA topology (Fig. 2b) and for both the MEC (Fig. 2c) and EEC (Fig. 2d) optimization of the SEA+UPS topology.

1) Phase shift of mechanical peak power: Mechanical peak power is reduced in all cases by storing some of the negative power resulting from controlled dorsiflexion in the spring and releasing it during push-off, when the highest output power is required. The parallel spring provides a power to the output which roughly follows the required biological output power. As a result, in the PEA case, the peak in mechanical peak power is slightly delayed. Conversely, a series spring shifts the power peak to terminal stance (30-50% GC). This will be explained in Section III-D.

2) Power peaks in swing: During swing, the only load seen by the prosthesis is the inertia of the foot, which is relatively low. As a result, almost no mechanical power is consumed during this phase of the gait cycle. Electrically, however, we observe large power peaks in the swing phase, especially for the SEA. These peaks have also been observed experimentally on SEA-driven prostheses such as the SPARKy 1 prosthesis [2] and the CYBERLEGS α-prosthesis [18]. They are caused by the reflected inertia of the drivetrain, which is related to its capability of producing torque. Parallel elastic elements reduce the torque required from the motor, whereas series elastic elements only have an impact on the motor speed. As a result, a higher gear ratio and/or a larger motor will be needed for the SEA, which will therefore have a higher reflected drivetrain inertia. Indeed: the EEC optimizations yield a reflected inertia of 0.960 kgm² for the PEA and SEA+UPS, while the reflected drivetrain inertia of the SEA is 3.40 kgm². This inertia is much higher than that of the human foot (around 0.035 kgm² [16]) and therefore probably that of the prosthesis. Consequently, the inertial torques due to the reflected drivetrain inertia will dominate the energy consumption during swing.

3) Power peaks due to interacting springs (SEA+UPS): Another important issue is the strong power peak at around 55% gait cycle in the SEA+UPS (EEC) simulation caused by the interaction between the parallel and series spring. Recall that the unidirectional parallel spring is represented by (3). The second derivative of this equation, $\ddot{T}_s$, is a pulse at $\theta =$

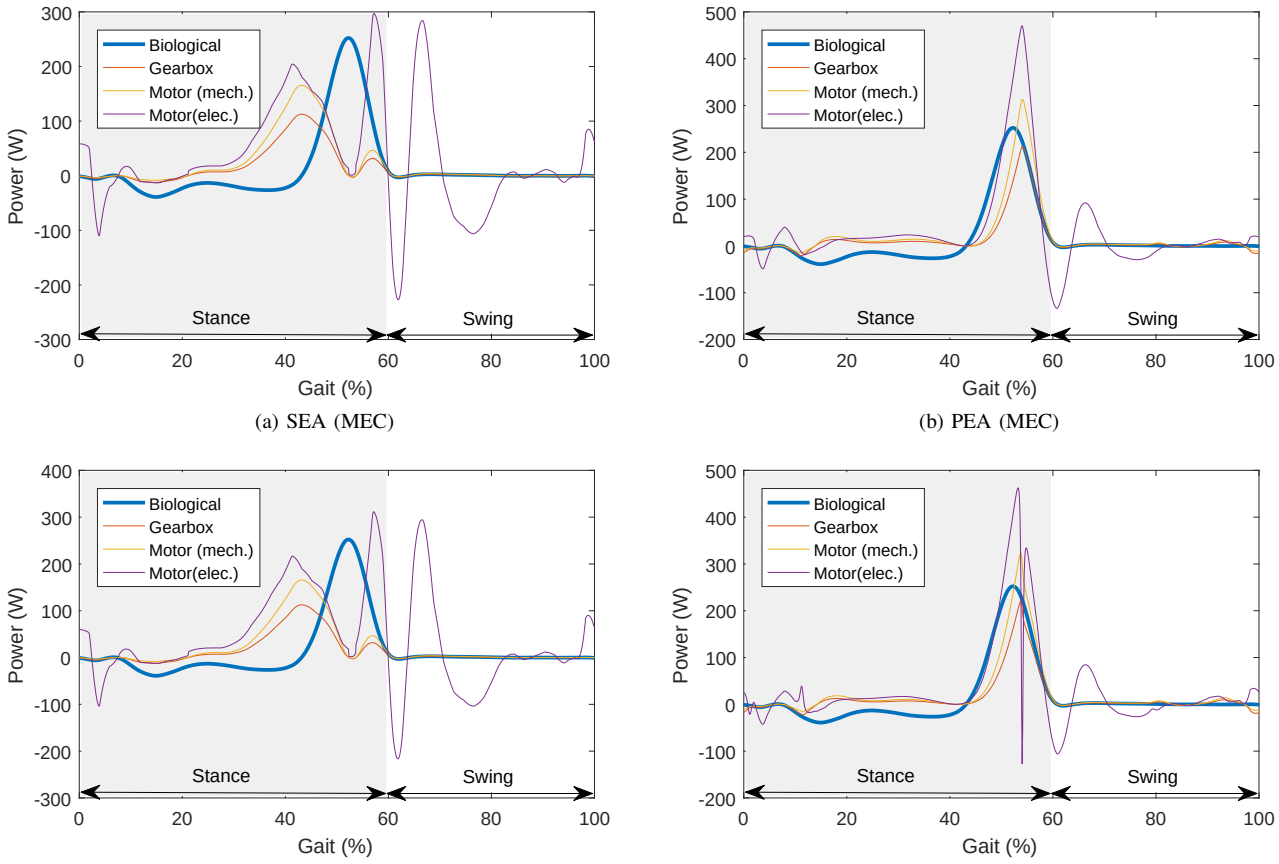

(a) SEA (MEC)

(b) PEA (MEC)

(c) SEA+UPS (MEC)

(d) SEA+UPS (EEC)

Fig. 2: Power flows for the different optimization criteria for different types of elastically actuated ankle prostheses. The required (biological) output power, obtained from Winter data [16], is shown in blue. Inertial torques due to the reflected drivetrain inertia dominate the energy consumption during swing.

θ_{eq}. Because the motor's acceleration is given by

$$\ddot{\theta}_m = n \cdot \left(\frac{\ddot{T} + \ddot{T}_s}{k_s} + \ddot{\theta} \right) \tag{14}$$

maintaining a continuous output speed when the parallel spring is (dis)engaged will require a strong acceleration from the motor. The accelerating inertia of the drivetrain will cause a high peak current and lead to a peak in motor power at 54% GC (EEC). Also note that, according to (14), the power peak increases with decreasing series spring stiffness. This explains why the EEC optimization maximizes the series spring stiffness of the SEA+UPS.

C. Motor efficiency maps

Another interesting tool for the analysis of an actuator's efficiency are motor efficiency maps. By plotting the operating points of the motor on such an efficiency map, one can visualize how efficiently the motor is used during the gait cycle. Efficiency maps for the PEA and SEA designs resulting from the EEC optimization are shown in Fig.3, along with two motor trajectories. The first is based on the motor shaft torque T_m, which is not influenced by drivetrain inertia. The second is based on the motor torque with drivetrain inertia included, $T_m + J_m \ddot{\theta}_m$. As seen in the figure, drivetrain inertia has a strong effect on the operating points of the motor. Motor torques are much higher, being pushed far beyond the continuous operating limits of the motor (white). This is especially the case for the SEA, which has a higher drivetrain inertia. Moreover, many of the operating points lie in regions with poor efficiency. As a result, the actual efficiency of the motor (SEA: 64%, PEA: 71%) is considerably lower than the catalog efficiency (SEA: 94%, PEA: 91%). Note that the PEA makes more efficient use of its motor, although the motor itself is less efficient than the one of the SEA.

D. Torque-angle characteristic

In the stance phase, the highest torques occur due to the spring-like load imposed on the ankle by the ground reaction forces. In comparison, inertial effects are negligible - at least when the drivetrain is taken out of consideration. Consequently, the torque-angle characteristic of the ankle can be used as a powerful design tool for the optimization of series and parallel springs during stance.

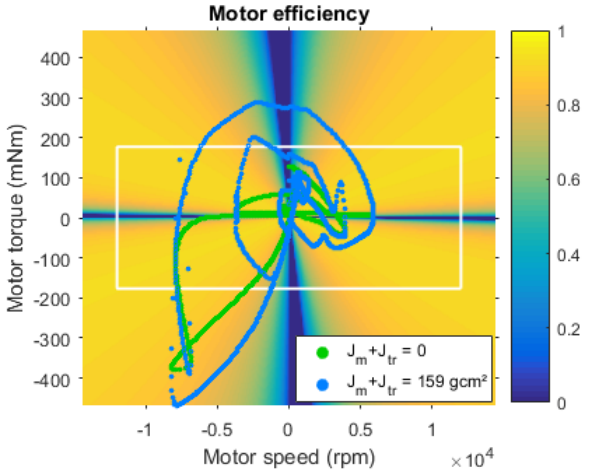

(a) PEA

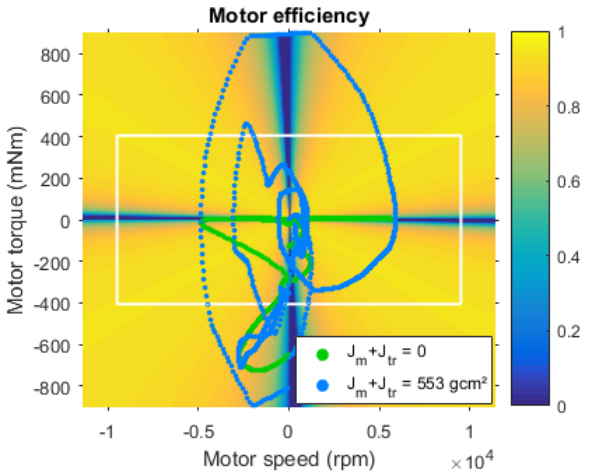

(b) SEA

Fig. 3: Four-quadrant efficiency maps for the EEC-optimized PEA and SEA designs. White lines indicate the boundaries set by the maximum motor speed $\dot{\theta}_{max}$ and the maximum continuous torque $T_{m,max,cont}$. The actual motor trajectory, which takes drivetrain inertia into account, is plotted in blue; the motor trajectory based on the torque on the motor shaft, not influenced by drivetrain inertia, is plotted in green. Drivetrain inertia appears to have a considerable influence on the torque delivered by the motor, especially for the SEA.

Fig. 4 shows the torque-angle characteristic of the human ankle for walking gait at a natural cadence. In Fig. 4a, the parallel spring characteristic from the EEC optimization for the PEA is overlaid. At the equilibrium angle of -1°, the parallel spring characteristic crosses the angle axis. Below this angle, no more torque is provided by the parallel spring. If the slope of the parallel spring matches that of the torque-angle characteristic, no torque will be delivered by the motor. In Fig. 4a, for example, it can be seen that the parallel spring delivers most of the torque during loading midstance and terminal stance (10-50% GC). During pre-swing (50-60% GC), the motor provides additional torque to make up for the remainder of the required output torque.

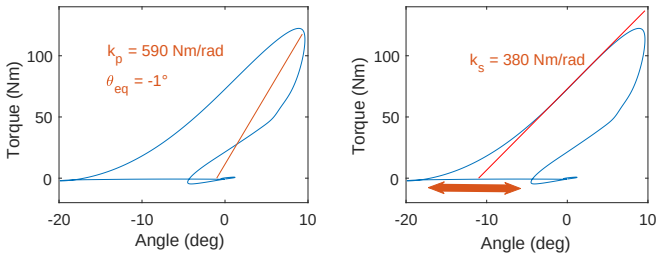

(a) PEA (b) SEA

Fig. 4: Torque-angle plot of the ankle for natural cadence of a healthy subject. Typical optimized values for (a) a unidirectional parallel spring and its equilibrium angle and (b) a series spring are shown in red. The intercept of the parallel spring is fixed, whereas that of the series spring is constantly changed by the motor.

In Fig. 4b, the optimized series spring characteristic from the MEC optimization for the SEA is shown. Unlike for the PEA, the SEA spring does not have a fixed angle-axis intercept (equilibrium angle), as the opposite end of the spring is no longer fixed to the ground. Instead, it is connected to the electric motor, which constantly changes the angle-axis intercept. When the slope of the series spring matches that of the torque-angle characteristic, the motor will provide torque without moving. In other words, the speed of the motor is reduced, and the electric motor's energy consumption is lowered. As illustrated in Fig. 4b, the optimized spring stiffness of 380 Nm/rad enables the motor to operate at near-zero speed during the pre-swing phase (50-60% GC). This is confirmed by Fig. 2a, which displays low mechanical power during this particular phase.

IV. Discussion

All the optimizations presented in this paper were based on inverse dynamics. As discussed in the introduction, there are several advantages to optimizing active ankle prostheses with series and parallel elastic elements in the electrical domain. Nevertheless, this approach also has some disadvantages.

First, the calculated currents and voltages can only be accurate if the drivetrain is modeled correctly [17]. Unfortunately, speed- and load-dependent efficiencies of motors and gearboxes are difficult to model based on catalog information alone. The determination of friction in the drivetrain is even more difficult, as it is affected by many variables such as temperature, lubrication, alignment and bearing selection. As a result, the calculations in the electrical domain, despite being more detailed, will also introduce additional uncertainties.

Secondly, in an SEA, discontinuous events require fast motion from the actuator. Such discontinuities occur because of Coulomb friction [19] or, as explained in section II-A, at the engagement of a unidirectional parallel spring. The discontinuities give rise to high peak currents and, consequently, high electrical power peaks. In an optimization based on mechanical power, these peaks are not observed

because motor dynamics are not taken into account. Note that, in practice, these currents may not be reached because of the limited bandwidth of the electric motor. The output of the actuator will then deviate from the desired force output. For active ankle prostheses, small deviations are often considered acceptable. In fact, real gait patterns often differ considerably from averaged gait data [16], so imposing perfect tracking makes little sense. Entirely discarding solutions which bring the electric motor into saturation, as done in our optimization (see section II-B), may thus impose too high demands on the actuator in terms of bandwidth than strictly needed.

Another reason why the actual actuator may deviate from the imposed trajectory is the bandwidth of the controller. A full characterization of the actuator would require a dynamic simulation of the closed-loop system, including both the actuator and its controller. In [20], the authors took this approach to optimize the stiffness of an SEA. They demonstrated that the energy consumption and peak power depends on the chosen controller – but also on the allowable tracking error. Here, too, the authors found a trade-off between low peak power and adequate tracking.

V. Conclusion

In this paper, we discussed how the design optimization of active ankle prostheses with elastic elements can benefit from calculating their electrical energy consumption. The gear ratio and springs of an SEA, PEA and SEA with unidirectional parallel spring were optimized by minimizing mechanical and electrical energy consumption. The PEA used a smaller motor than the SEA which, moreover, was used more efficiently: the actual efficiency of the PEA's motor was 71%, compared to 64% for the SEA. A further analysis of the results revealed two important differences between electrical and mechanical energy consumption. First, drivetrain inertia causes additional power peaks during swing. Second, the (dis)engagement of the unidirectional parallel spring requires fast movement from the motor, resulting in high power peaks.

We also presented a novel interpretation of the torque-angle plot, which relates spring stiffness to reduction of motor speed in the SEA and the reduction of motor torque in the PEA. This interpretation enabled us to explain the mechanical power profiles of the optimized SEA and PEA. We argued that the stiffness of the SEA should be tuned to the ankle's quasi-stiffness in pre-swing, as the torque-angle plot is most linear in this phase and, hence, the highest reductions in peak power can be achieved.

Our results indicate that optimizing for mechanical energy consumption can yield energy-efficient elastic actuator designs. Nevertheless, we found calculations in the electrical domain to be essential, not only for minimizing energy consumption, but also for maximizing bandwidth. This optimization principle will be applied in new iterations of our department's active prostheses of the AMPfoot and CYBERLEGs family.

References

[1] T. Verstraten, P. Beckerle, R. Furnémont, G. Mathijssen, B. Vanderborght, and D. Lefeber, "Series and parallel elastic actuation: Impact of natural dynamics on power and energy consumption," *Mechanism and Machine Theory*, vol. 102, pp. 232–246, 2016.

[2] J. K. Hitt, T. G. Sugar, M. Holgate, and R. Bellman, "An active foot-ankle prosthesis with biomechanical energy regeneration," *Journal of Medical Devices*, vol. 4, no. 1, p. 011003, 2010.

[3] L. Flynn, J. Geeroms, R. Jimenez-Fabian, B. Vanderborght, N. Vitiello, and D. Lefeber, "Ankle-knee prosthesis with active ankle and energy transfer: Development of the CYBERLEGs alpha-prosthesis," *Robotics and Autonomous Systems*, vol. 73, pp. 4 – 15, 2015, wearable Robotics.

[4] F. Sup, H. A. Varol, J. Mitchell, T. J. Withrow, and M. Goldfarb, "Preliminary evaluations of a self-contained anthropomorphic transfemoral prosthesis," *IEEE/ASME Transactions on Mechatronics*, vol. 14, no. 6, pp. 667–676, Dec 2009.

[5] F. Gao, Y. Liu, and W. H. Liao, "A new powered ankle-foot prosthesis with compact parallel spring mechanism," in *2016 IEEE International Conference on Robotics and Biomimetics (ROBIO)*, Dec 2016, pp. 473–478.

[6] S. K. Au, J. Weber, and H. Herr, "Powered ankle–foot prosthesis improves walking metabolic economy," *IEEE Transactions on Robotics*, vol. 25, no. 1, pp. 51–66, Feb 2009.

[7] R. Jimenez-Fabian, J. Geeroms, L. Flynn, B. Vanderborght, and D. Lefeber, "Reduction of the torque requirements of an active ankle prosthesis using a parallel spring," *Robotics and Autonomous Systems*, vol. 92, no. Supplement C, pp. 187 – 196, 2017.

[8] M. Grimmer, M. Eslamy, and A. Seyfarth, "Energetic and peak power advantages of series elastic actuators in an actuated prosthetic leg for walking and running," *Actuators*, vol. 3, no. 1, p. 1, 2014.

[9] M. Grimmer, M. Eslamy, S. Gliech, and A. Seyfarth, "A comparison of parallel- and series elastic elements in an actuator for mimicking human ankle joint in walking and running," in *Robotics and Automation (ICRA), 2012 IEEE International Conference on*, May 2012, pp. 2463–2470.

[10] M. Eslamy, M. Grimmer, and A. Seyfarth, "Effects of unidirectional parallel springs on required peak power and energy in powered prosthetic ankles: Comparison between different active actuation concepts," in *Robotics and Biomimetics (ROBIO), 2012 IEEE International Conference on*, Dec 2012, pp. 2406–2412.

[11] S. Wang, W. van Dijk, and H. van der Kooij, "Spring uses in exoskeleton actuation design," in *Rehabilitation Robotics (ICORR), 2011 IEEE International Conference on*, June 2011, pp. 1–6.

[12] P. Beckerle, J. Wojtusch, A. Seyfarth, O. V. Stryk, and S. Rinderknecht, "Analyzing and considering inertial effects in powered lower limb prosthetic design," in *Rehabilitation Robotics (ICORR), 2015 IEEE International Conference on*, Aug 2015, pp. 325–330.

[13] D. Paluska and H. Herr, "The effect of series elasticity on actuator power and work output: Implications for robotic and prosthetic joint design," *Robotics and Autonomous Systems*, vol. 54, no. 8, pp. 667 – 673, 2006, morphology, Control and Passive Dynamics.

[14] T. Verstraten, G. Mathijssen, J. Geeroms, L. Flynn, B. Vanderborght, and D. Lefeber, *On the Importance of a Motor Model for the Optimization of SEA-driven Prosthetic Ankles*. Cham: Springer International Publishing, 2017, pp. 403–407.

[15] T. Verstraten, J. Geeroms, G. Mathijssen, B. Convens, B. Vanderborght, and D. Lefeber, "Optimizing the power and energy consumption of powered prosthetic ankles with series and parallel elasticity," *Mechanism and Machine Theory*, vol. 116, pp. 419 – 432, 2017.

[16] D. A. Winter, *Biomechanics and motor control of human movement*, 4th ed. John Wiley & Sons, 2009.

[17] T. Verstraten, R. Furnémont, G. Mathijssen, B. Vanderborght, and D. Lefeber, "Energy consumption of geared DC motors in dynamic applications: Comparing modeling approaches," *IEEE Robotics and Automation Letters*, vol. 1, no. 1, pp. 524–530, 2016.

[18] J. Geeroms, L. Flynn, R. Jimenez-Fabian, B. Vanderborght, and D. Lefeber, "Energetic analysis and optimization of a MACCEPA actuator in an ankle prosthesis," *Autonomous Robots*, pp. 1–12, 2017.

[19] P. E. Dupont, "The effect of coulomb friction on the existence and uniqueness of the forward dynamics problem," in *Proceedings 1992 IEEE International Conference on Robotics and Automation*, May 1992, pp. 1442–1447 vol.2.

[20] O. B. Farah, Z. Guo, C. Gong, C. Zhu, and H. Yu, "Power analysis of a series elastic actuator for ankle joint gait rehabilitation," in *2015 IEEE International Conference on Robotics and Automation (ICRA)*, May 2015, pp. 2754–2760.